Journal of Physics D: Applied Physics

PAPER • OPEN ACCESS

Improving luminescence response in $ZnGeN_2$/GaN superlattices: defect reduction through composition control

To cite this article: Moira K Miller *et al* 2024 *J. Phys. D: Appl. Phys.* **57** 375106

OPEN ACCESS
IOP Publishing
Journal of Physics D: Applied Physics
J. Phys. D: Appl. Phys. **57** (2024) 375106 (8pp)
https://doi.org/10.1088/1361-6463/ad54ce

Improving luminescence response in $ZnGeN_2$/GaN superlattices: defect reduction through composition control

Moira K Miller[1], David Diercks[1] and M Brooks Tellekamp[2,*]

[1] Colorado School of Mines, Golden, CO, United States of America
[2] National Renewable Energy Laboratory, Golden, CO, United States of America

E-mail: brooks.tellekamp@nrel.gov

Received 10 March 2024, revised 17 April 2024
Accepted for publication 6 June 2024
Published 24 June 2024

Abstract

Color-mixed (cm) light-emitting diodes (LEDs) are theoretically the most efficient white light emitters, projected to improve white light luminous efficacy by 34% compared to incumbent phosphor converted LEDs. Since white light technology is pervasive and essential, small improvements in LED technology can result in energy savings. However, cm-LEDs are not yet realized due to poor efficacy in green and amber emitting materials, a spectral region colloquially referred to as the Green Gap. $ZnGeN_2$ is nearly isostructural and closely lattice-matched to GaN and can be heteroepitaxially integrated with existing GaN devices; $ZnGeN_2$/GaN hybrid structures are theorized to emit green (~530 nn) light with a spontaneous emission rate 4.6–4.9 times higher than traditional InGaN LEDs when incorporated into III-N LED structures. In this report we demonstrate the molecular beam epitaxy (MBE) growth of GaN and $ZnGeN_2$ superlattices, an important step towards realizing multiple quantum well structures required for efficient LEDs. Elemental analysis, including atom probe tomography, shows that Ga and Ge are observed in both $ZnGeN_2$ and GaN layers, degrading the structural uniformity. The lack of elemental abruptness also leads to increased defect luminescence and reabsorption of band edge luminescence. The source of unintentional Ga distributed throughout the $ZnGeN_2$ layers was identified as excess flux escaping from around the closed MBE shutter. The source of unintentional Ge, which tended to incorporate as a single delta-doped layer in GaN, was identified as Ge riding along the cyclical metal-rich Ga adlayer used for high quality GaN, incorporating during subsequent nitrogen-rich growth step. Modifying the growth strategy results in improved structural quality, elemental abruptness, and luminescence response. This realization of structurally and elementally abrupt interfaces demonstrates the potential of heteroepitaxially integrated binary and ternary nitrides for energy-relevant devices.

Supplementary material for this article is available online

Keywords: $ZnGeN_2$, GaN, EDS, APT, PL, superlattice, MBE

* Author to whom any correspondence should be addressed.

1. Introduction

Color-mixed (cm) light-emitting diode (LED) technologies are projected to increase luminous efficacy (lm/W) by 34% when compared to traditional phosphor-converted (pc) LEDs according to a 2050 U.S. Department of Energy target [1]. However, pc-LEDs are the industry standard for white light because it is currently more efficient to down-convert low In-content blue LEDs than it is to use direct-emitting green and amber LEDs with higher In content. This down conversion process is inherently lossy- energy is dissipated to heat to convert to the longer wavelengths of light. cm-LEDs, which use individual emitters for blue, green, red, and amber light, are theoretically the most efficient method for generating white light. These cm-LEDs have not yet been realized due to the Green Gap, a spectral region from 500-600 nm with significantly lower demonstrated efficiency than blue III-N or red III-V LEDs [1]. The Green Gap results from fundamental materials limitations in the (In,Ga)N system, including alloy immiscibility and the large polarization and lattice mismatch between the two binary compounds [2–4].

One solution to improve green or amber LED efficiency in nitride semiconductors is an alternative emitter material with an appropriate bandgap and a more favorable lattice match to GaN when compared to InGaN alloys. One proposed material is the heterovalent ternary $ZnGeN_2$, which is nearly lattice-matched to GaN (~0.2% lattice mismatch) [5]. $ZnGeN_2$ is theorized to have a bandgap tunable with disorder or band engineering into the green and amber regions, with a spontaneous emission rate 4.6–4.9 times higher than traditional InGaN LEDs when incorporated into current III-N LED structures [6–10]. Cation-ordered $ZnGeN_2$ is theorized to have a type-II band offset with GaN, although small amounts of cation disorder are theorized to decrease the band gap enough to result in a type-I band offset [8]. $ZnGeN_2$ epitaxy has already been demonstrated by metal-organic chemical vapor deposition (MOCVD) [11–18], sputtering [7, 19], and molecular beam epitaxy (MBE) [5, 20, 21]. Heterostructures of $ZnGeN_2$ and GaN have been demonstrated by MBE and MOCVD, and heterostructures with GaN and InGaN have been demonstrated by MOCVD, although indium was observed to diffuse broadly across the entire heterostructure [15, 21]. To achieve highly efficient LEDs, superlattices (multiple quantum well structures) with abrupt interfaces are required but have not been demonstrated in the III-N/II-IV-N_2 material system.

This study investigates $ZnGeN_2$/GaN superlattices to explore the effects of multiple heterointerfaces on structure, compositional purity, and interfacial abruptness. We demonstrate growth of five repeating unit superlattices of $ZnGeN_2$ and GaN on commercial GaN templates. We observe unintentional incorporation of Ge in GaN and Ga in $ZnGeN_2$, and present growth strategies to reduce unintentional impurities in each layer. Spatially resolved composition is correlated with structural uniformity which is observed to impact the luminescence response of the superlattice. Improving the compositional abruptness results in improved structural uniformity, decreased defect luminescence, and brighter band edge luminescence due to reduced parasitic absorption.

2. Experimental section

GaN and $ZnGeN_2$ were grown by MBE on n-type GaN templates (3LCorp, Si-doped, 6 μm thick), using previously published methods [21]. The substrates were cleaned *in situ* by three Ga polishing cycles, used to remove the surface oxide. In this process the GaN surface is covered with Ga and then heated to form and desorb Ga_2O along with excess Ga [22]. Two samples were investigated, each targeting five repeating units of 2.6 nm $ZnGeN_2$/13 nm GaN. Metal-modulated epitaxy (MME) was used to grow GaN with a III/V ratio of 1.8, 10/10 s Ga shutter open/closed times, and a substrate temperature of 600 °C [23]. Three MME cycles were required to deposit the 13 nm GaN layers. $ZnGeN_2$ was grown in a nitrogen-rich adsorption-controlled regime with a Zn overpressure and a substrate temperature of 400°C. The substrate temperature was calibrated to the melting point of Al using a pyrometer. Each growth followed the same structure: a 130 nm GaN regrowth was deposited on the Ga-polished n-GaN template, followed by five repeating superlattice units, and capped with 130 nm GaN (see figure 1).

X-ray diffraction (XRD) and reflection high-energy electron diffraction (RHEED) were used to investigate structural quality. *In situ* RHEED was performed using a 20 keV Staib Instruments electron gun and a CCD camera/phosphor screen. Symmetric XRD was performed in a triple-axis geometry using a SmartLab Rigaku XRD with an incident beam Ge(220) 2-bounce monochromator and diffracted beam Ge(220)×2 analyzer crystal. Reciprocal space maps (RSMs) were taken using a Panalytical MRD-Pro sourcing Cu-kα radiation with a parabolic mirror and Ge (400) 4-bounce monochromator. The two-dimensional CCD detector has a 2θ resolution of 0.0025°.

Photoluminescence (PL) was used to investigate optical properties at low temperature (4 K). A 325 nm He–Cd laser was used for excitation filtered to 1 mW incident power. Data was collected with a 0.3 m spectrometer and Si-CCD detector with a UV sensitive coating. A white-light standard (from the National Institute of Standards and Technology) was used to correct for wavelength-dependent detector efficiency.

Specimens for atom probe tomography (APT) and transmission electron microscopy (TEM) were prepared using lift-out focused ion beam (FIB) methods on a Tescan S8252G FIB/scanning electron microscope instrument [24, 25]. TEM and scanning TEM (STEM) imaging were performed on a Thermo Fisher Scientific Talos F200X instrument using a 200 keV accelerating voltage. Scanning transmission energy dispersive x-ray spectroscopy (STEM-EDS) maps were collected at various regions around the layered structure and processed using Bruker's Esprit 1.9 software. APT specimens were prepared such that they could also be imaged in the TEM before and after APT analysis [26]. APT data were collected via laser pulsing on a Cameca LEAP 4000X Si instrument at

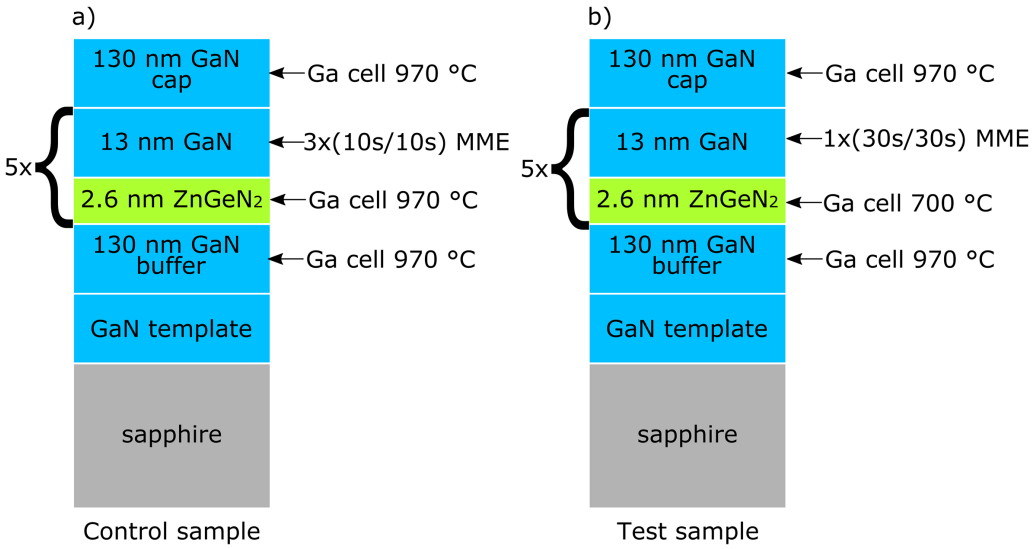

Figure 1. Control sample (a) and test sample (b) used to identify sources of unintentional Ga incorporation into $ZnGeN_2$ and Ge incorporation into GaN. They have identical structures with noted growth parameters modified during superlattice growth. The superlattice region is indicated by curly brackets. The test sample decreases the idle shuttered Ga temperature during $ZnGeN_2$ growth and utilizes a single longer MME cycle (30 s shutter open/30 s shutter closed), while the control sample does not change the Ga temperature and uses three shorter MME cycles (10 s shutter open/10 s shutter closed).

a base temperature of 51.4 K and flight path length of 90 mm. The laser pulse energies ranged from 9 to 90 fJ with pulse repetition rates of either 625 or 833 kHz. APT reconstructions were generated and analyzed in Cameca's IVAS 3.6.18 software. The TEM images (SI figure 1) were used to inform the reconstruction parameters following the method of Diercks and Gorman [27].

3. Results

Due to the disparate growth temperatures for $ZnGeN_2$ (400 °C) and GaN (600 °C) synthesis by MBE growth was interrupted between layers for a temperature ramp with all shutters closed, i.e. no direct nitrogen flux. $ZnGeN_2$ synthesis was initiated as soon as the substrate temperature reached 400 °C. To avoid decomposition of the $ZnGeN_2$, the GaN layer was deposited upon temperature ramping, opening the shutters at 475 °C and continuing to ramp at 200 °C/min to 600 °C. Typically the first 6 nm – 7 nm of the GaN layer were deposited during the temperature ramp, with the remaining thickness grown at 600 °C. The control sample (figure 1(a)) was grown with Ga at the GaN growth temperature (~970 °C) with a closed shutter during $ZnGeN_2$ growth layer. The test sample (figure 1(b)) was grown with the Ga cell cooled to 700 °C degrees and a closed shutter during $ZnGeN_2$ layer growth. The Ga cell was cooled during $ZnGeN_2$ growth to investigate the source of unintentional Ga in $ZnGeN_2$ layers. The GaN superlattice layer for the test sample was grown using a single MME cycle of identical thickness (30 s shutter open/30 s shutter closed), compared to three MME cycles (10 s shutter open/10 s shutter closed) for the control sample, to investigate Ge incorporation in the GaN layers. Metal rich growth of GaN on $ZnGeN_2$ is important to prevent 3D island growth due to the unfavorable surface energy configuration since $ZnGeN_2$ grows in a 2D layer-by-layer growth mode when nucleated on GaN (as seen by RHEED oscillations). In other words $ZnGeN_2$ can wet the GaN surface, but GaN will not wet the $ZnGeN_2$ surface without the presence of a metallic Ga adlayer [28].

The surface quality and crystallinity of each sample were monitored by RHEED. RHEED patterns for the first and last $ZnGeN_2$ superlattice layers, taken at the end of each layer growth, are shown in figure 2(b). RHEED oscillations, indicative of 2D layer by layer growth, were used to monitor the $ZnGeN_2$ layer thickness (figure 2(a)). The RHEED pattern of the GaN buffer prior to growth shows strong Kikuchi lines from inelastic bulk scattering that diminish in intensity at the end of growth. A (2×2) surface reconstruction is observed indicative of a flat Ga-polar surface. We observe streaky RHEED patterns throughout the growth of all layers, indicative of a flat surface (complete set of RHEED images available in SI figure 2). However, the diffraction intensity tends to decrease during each $ZnGeN_2$ layer, consistent with increasing disorder. The intensity is regained upon each GaN layer growth, and (2×2) reconstructions were instantaneously visible for each GaN layer. There were no significant changes observed by RHEED when comparing the test sample to the control sample.

Symmetric XRD around the (0002) peak is shown in figure 3(a). The control sample shows weak 1st order superlattice reflections with a superlattice period of approximately 13.5 nm. The test sample shows up to 3rd order superlattice peaks with a superlattice period of 15 nm. The set of Pendellösung fringes with highest frequency is associated with the GaN cap (130 nm) in each XRD pattern. RSMs around the (1 0 $\bar{1}$ 5) reflection, shown in figures 3(b) and (c), were

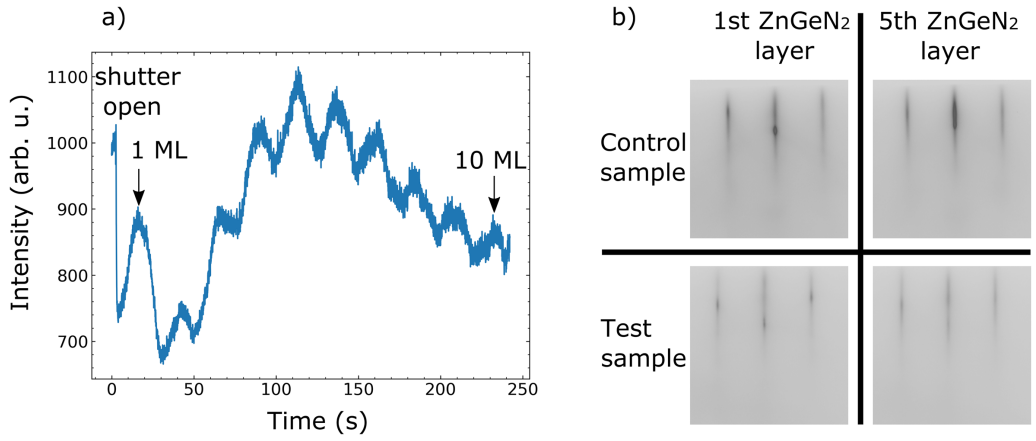

Figure 2. Reflection high-energy electron diffraction (RHEED) of the control and test samples showing layer by layer growth and smooth surfaces. (a) RHEED intensity (arbitrary units) versus time (s) for the duration of the first $ZnGeN_2$ layer in the test sample. Each oscillation shows the completion of one monolayer (2.6 Å) of $ZnGeN_2$. (b) RHEED images for the 1st and last $ZnGeN_2$ layers for both the control and test samples.

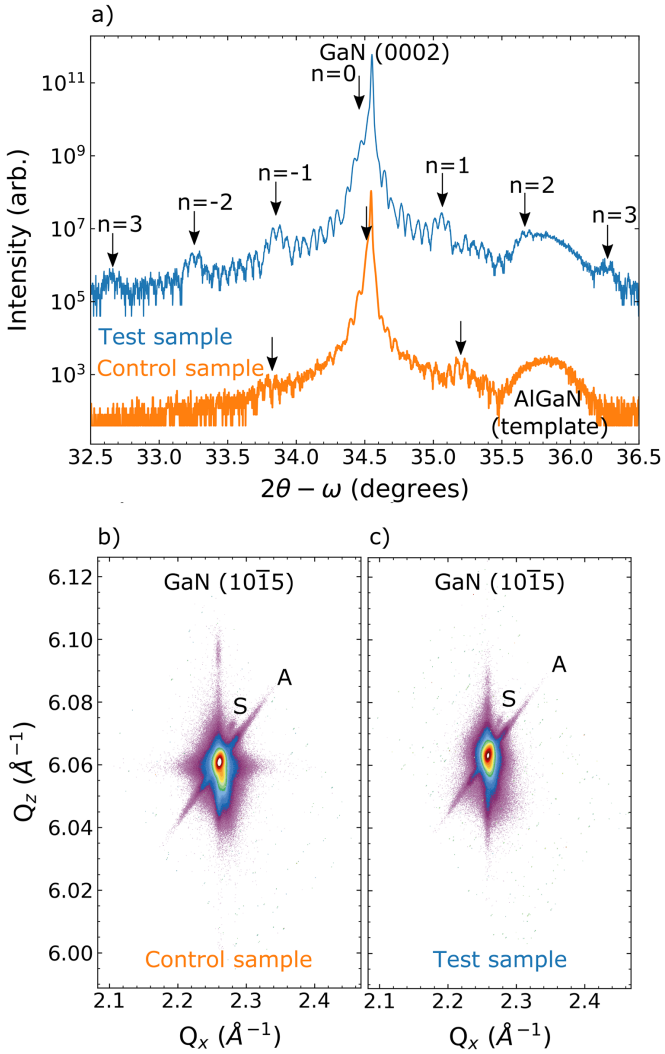

Figure 3. XRD structural characterization of the control and test structures. (a) Symmetric XRD of the control sample (orange) and test sample (blue). Asymmetric reciprocal space maps (RSM) around the (1 0 $\bar{1}$ 5) reflection for the control sample (b) and test sample (c) with the sample (S) and analyser (A) streak artifacts labelled. The AlGaN observed by XRD is due to GaN nucleation onto sapphire during commercial growth of the GaN template.

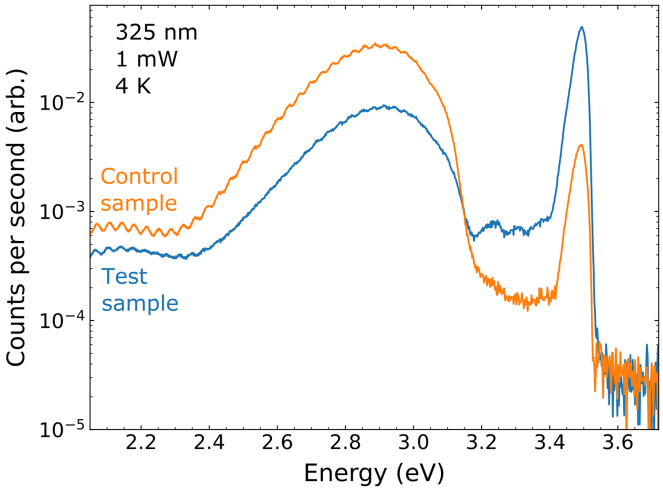

Figure 4. Low temperature photoluminescence (PL) of the control sample (orange) and test sample (blue). The defect luminescence band can be seen in both samples centered around 2.9 eV. The GaN and cation-ordered $ZnGeN_2$ band edge signals overlap at 3.5 eV. The peak at 2.15 eV is yellow band luminescence from the GaN template.

also obtained to analyze strain and defects. Lateral broadening around the GaN (1 0 $\bar{1}$ 5) is indicative of dislocations along the growth direction which act to decrease the lateral coherence length and increase broadening in reciprocal space [21]. Elongated features in Q_z represent the crystal truncation rod.

Low-temperature (4 K) PL was used to investigate the impact of unintentional impurities on optical properties (figure 4). The defect luminescence that can be seen in both samples as a broad feature centered around 2.9 eV originates from the $ZnGeN_2$ layer and overlaps a Zn:GaN impurity transition [21]. The 2.9 eV $ZnGeN_2$ peak was identified as a free-to-bound defect transition in a previous study where $ZnGeN_2$ was grown directly on AlN substrates without any GaN, noting that the same peak energy is also associated with a donor-acceptor pair in Zn:GaN [20, 29]. In a prior study, we used low temperature power dependent PL to differentiate the two overlapping luminescence signals [21]. A blue shift of the 2.9 eV peak with increasing power is characteristic of a donor-acceptor pair, while the absence of such shift is associated with a free-to-bound transition in $ZnGeN_2$ that may originate from either Zn_{Ge} antisites or Ga_{Ge} substitution. The control sample showed a clear blue-shift with increasing power; however, the test sample did not show any evidence of blue shifting over 3-orders of magnitude laser power (see SI figure 5). Thus, it appears that improvements to unintentional Ge and Ge incorporation have also reduced the unintentional Zn doping of GaN. The GaN band-edge signal is present in both samples and overlaps the band edge signal (3.5 eV) for cation-ordered $ZnGeN_2$. [30] The peak at 2.15 eV is yellow band luminescence from the GaN template.

APT and STEM-EDS were performed to investigate the interface abruptness and layer composition. Figure 5 shows comparative line scans from the APT reconstructions (directly through the middle of the reconstruction cone using a 33 nm diameter cylinder) for the control sample (a) and the test sample (c). The EDS line scans and elemental mapping can be found in SI figure 3. First, we note that for APT the detection sensitivity for cation:nitrogen ratio is proportional to the local electric field, leading to apparent variations in cation:N stoichiometry. For EDS, absorption of the low energy nitrogen x-ray lines can lead to underestimations of nitrogen content when using the Cliff-Lorimer method employed here [31]. Since we are concerned primarily with the cation distribution, we focus on those for the analyses. In both samples the five $ZnGeN_2$ layers can be clearly seen in both the APT and EDS plots.

APT shows that the control sample has unintentional incorporation of Ga and Ge outside of their expected layers. In the control sample, Ga (red trace) is found in the $ZnGeN_2$ layers at about 15%–25%, indicative of unintentional incorporation or alloying of Ga with the $ZnGeN_2$. Also visible by APT is Ge incorporation into the GaN layers. Small Ge peaks are visible within the GaN layers, about 4–5 nm into each GaN layer (dark blue peaks in the GaN layers; indicated with blue arrows). The Ge incorporation layer is corroborated through high-angle annular dark-field imaging (HAADF) approximately 5 nm above the preceding $ZnGeN_2$ layer. A small portion of the HAADF for each sample is shown in figure 5, aligned to the superlattice layers in the APT plot, also indicating Ge incorporation with blue arrows (STEM-EDS and full HAADF images in SI figures 3 and 4).

4. Discussion

Determining the source of unintentional Ga and Ge incorporation is essential to integrate $ZnGeN_2$ into III-N heterostructures and devices such as LEDs. We first hypothesized that stray Ga flux from the hot Ga cell at GaN growth temperature incorporated into the $ZnGeN_2$ layers in the control sample. Noting that the GaN growth rate is approximately 25x faster than $ZnGeN_2$ growth rate and that MBE shutters do not provide 100% flux isolation, escaping flux from the Ga cell behind the closed shutter could be enough to incorporate at alloy level compositions. To test this hypothesis, we grew the test sample with the Ga cell cooled to 700 °C, rather than keeping it at GaN growth temperature during the $ZnGeN_2$ layers, to reduce stray flux and unintentional incorporation. Such alloying is not unexpected—there have been prior reports of intentional formation of $ZnGeN_2$-GaN alloys both at low GaN concentrations and at the 50% $ZnGeGa_2N_4$ composition [16–18].

The Ge in the GaN layers was found to incorporate in a discrete layer about about 4–5 nm after the $ZnGeN_2$ layer, or after one MME GaN cycle, appearing like a delta-doped layer by HAADF (SI figure 4). We hypothesized that the Ge was riding upon the Ga metal adlayer during the metal-rich step of the first MME cycle, and then incorporating into the GaN during the nitrogen-rich step. A similar effect has been observed for Ge and other dopants and impurities which do not incorporate during metal-rich GaN growth [32, 33]. To stop this migration of Ge, the GaN layer growth method for the test sample was switched from three 10/10 s open/closed MME cycles to

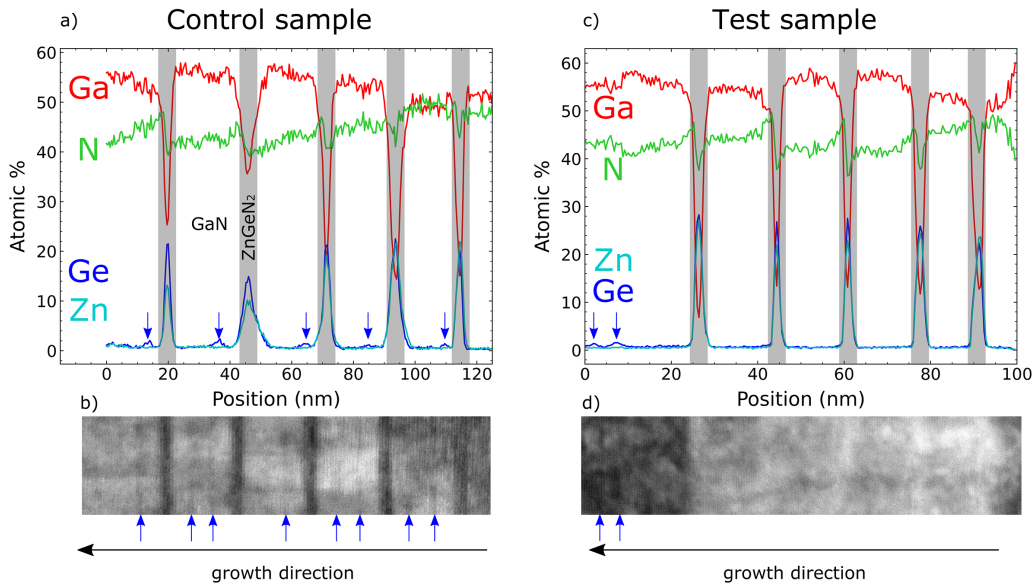

Figure 5. Atom probe tomography (APT) line profiles for the control (a) and test (c) samples. Plots show atomic % versus position within the superlattice region. Grey boxes indicate the $ZnGeN_2$ layers, with the GaN layers in between. Discrete spikes of Ge signal within the GaN layers are marked with blue arrows. The Ga signal does not drop to zero in the $ZnGeN_2$ layers. A portion of control (b) and test (d) sample HAADF rotated so superlattice layers align with the APT. Blue arrows also mark Ge incorporation.

one longer, 30/30 s open/closed MME cycle. This removed the opportunity for the residual Ge to incorporate into the GaN since there was no growth interrupt, while still growing the same GaN thickness.

Comparing the test and control samples, APT shows reduction in both Ge and Ga species outside of their respective layers, corroborating our hypotheses about incorporation in the control sample. As shown in figure 5(c), the Ga in the $ZnGeN_2$ layers is reduced from 15%–25% (control) to 8%–15% (test). The Ge peaks within the GaN layers have been completely eliminated to the resolution of the measurement. However, there are two Ge peaks visible in the GaN cap (marked with blue arrows in figures 5(c) and (d) when the MME growth cycle reverted to 10 s open and 10 s closed, confirming that incorporation of excess Ge into GaN only occurs during nitrogen-rich steps. The presence of a second Ge peak corresponding to the second MME cycle is indicative of Ge exceeding the solid solubility limit in GaN, suggesting that Ge continually accumulates during repeated heterolayer growth and is incorporated until the excess germanium is completely consumed by nitrogen-rich growth steps. The source of Ge is unknown at this time but could be due to $ZnGeN_2$ decomposition at GaN growth temperatures. Alternative strategies, such as immediate low growth temperature, nitrogen-rich GaN nucleation or temperature ramping under a Zn-overpressure could be successful future strategies to reduce this decomposition.

Structural characterization shows improved structural uniformity correlated with the improved compositional uniformity. Symmetric XRD scans show increased material quality for the test growth, with three satellite peaks clearly observed compared to one satellite peak in the control sample. Pendellösung fringes are clearer in the test sample indicating greater vertical coherence. RSMs of the test sample show that the GaN capping layer is less defective through decreased broadening in Q_x, indicating the test growth has fewer extended defects decreasing the lateral coherence length. Based on the width of the laterally broadened feature in Q_x the defect density in the five repeating unit superlattice film is not significantly different than the previously published double heterostructures, indicating that the additional superlattice interfaces do not significantly increase the Q_x broadening [20]. RHEED of both samples remains bright and streaky without a change in diffraction distance throughout the entire growth, confirming high-quality, commensurate growth of a 5-repeating superlattice layer structure, without significant loss in structural quality as the number of interfaces is increased (SI figure 2(b)).

PL (figure 4) found improvement in optical properties in the test sample with reduced unintentional incorporation of Ge and Ga. Three longitudinal-optical (LO) phonon replicas are visible in the test sample (blue), but not the control sample (orange), indicating that the crystalline and optical quality of the GaN cap is significantly improved. In contrast to previously published work, the LO phonon replicas are associated with GaN free exciton emission rather than a Zn:GaN acceptor bound exciton [20]. The increased band edge luminescence in the test sample compared to the control sample suggests some combination of decreased parasitic absorption by the $ZnGeN_2$ layer, increased luminescence from the GaN cap, and potentially band edge luminescence from $ZnGeN_2$. Decreased intensity of the 2.9 eV defect band in the test sample corroborates fewer defects and decreased parasitic absorption in the $ZnGeN_2$ layer. Overall,

the improvements in structural quality and superlattice layer abruptness result in measurable improvements to the PL spectra through increasing band edge signal and decreased defect luminescence.

In conclusion, we have demonstrated $ZnGeN_2$/GaN superlattices grown by MBE, methods to control unintentional incorporation in each heterolayer, and resulting improvements to the luminescence response. Structural and compositional analysis of both control and test samples reveal stray Ga flux and Ge incorporation during the nitrogen-rich MME stage to be the sources of unintentional impurity incorporation in $ZnGeN_2$ and GaN layers respectively. By controlling for these factors, the Ga concentration in $ZnGeN_2$ layers was reduced by 50%–60% compared to the control sample and Ge in the GaN layers was reduced to below the detection limit. PL confirms the impact of impurities on optical properties with the test sample having reduced defect signal and visible phonon replicas. The demonstration of superlattices with abrupt interfaces and control of unintentional impurities are important steps towards enabling hybrid III-N/II-IV-N_2 optoelectronic devices and establishes a path forwards towards highly efficient cm-LEDs.

Data availability statement

All data that support the findings of this study are included within the article (and any supplementary files).

Acknowledgments

This work was authored in part by the National Renewable Energy Laboratory, operated by Alliance for Sustainable Energy, LLC, for the U.S. Department of Energy (DOE) Under Contract No. DE-AC36-08GO28308. Funding provided by the U.S. Department of Energy Office of Energy Efficiency Building Technologies Office. The views expressed in the article do not necessarily represent the views of the DOE or the U.S. Government. The Tescan S8252G instrument was acquired through the support of the National Science Foundation (DMR-1828454). Some of the electron microscopy was performed in core facility RRID:SCR-022048 and the atom probe tomography was performed in RRID:SCR-023392, both of which are a part of Colorado School of Mines' Shared Instrumentation Facility.

Conflicts of Interest

The authors have no conflicts of interest to declare.

ORCID iDs

Moira K Miller https://orcid.org/0000-0001-5040-4685
David Diercks https://orcid.org/0000-0002-5138-0168
M Brooks Tellekamp https://orcid.org/0000-0003-3535-1831

References

[1] Pattison M, Hansen M, Bardsley N, Thomson G D, Gordon K, Wilkerson A, Lee K, Nubbe V and Donnelly S 2022 2022 solid-state lighting R&D opportunities
[2] Ho I and Stringfellow G 2021 Solid phase immiscibility in GaInN *Appl. Phys. Lett.* **69** 2701–3
[3] Yam F K and Hassan Z 2008 InGaN: an overview of the growth kinetics, physical properties and emission mechanisms *Superlattices Microstruct.* **43** 1–23
[4] Krames M R, Shchekin O B, Mueller-Mach R, Mueller G O, Zhou L, Harbers G and Craford M G 2007 Status and future of high-power light-emitting diodes for solid-state lighting *J. Disp. Technol.* **3** 160–75
[5] Tellekamp M B, Melamed C L, Norman A G and Tamboli A 2020 Heteroepitaxial integration of $ZnGeN_2$ on GaN buffers using molecular beam epitaxy *Cryst. Growth Des.* **20** 1868–75
[6] Schnepf R R *et al* 2020 Utilizing site disorder in the development of new energy-relevant semiconductors *ACS Energy Lett.* **5** 2027–41
[7] Melamed C L, Tellekamp M B, Mangum J S, Perkins J D, Dippo P, Toberer E S and Tamboli A C 2019 Blue-green emission from epitaxial yet cation-disordered $ZnGeN_{2-x}O_x$ *Phys. Rev. Mater.* **3** 051602
[8] Cordell J J, Miller M K, Tellekamp M B, Tamboli A, Tucker G J and Lany S 2022 Simulated structural and electronic properties of cation-disordered $ZnGeN_2$ *Phys. Rev. Appl.* **18** 064030
[9] Hyot B, Rollès M and Miska P 2019 Design of efficient type-II $ZnGeN_2/In_{0.16}Ga_{0.84}N$ quantum well-based red LEDs *Phys. Status Solidi* **13** 1900170
[10] Han L, Kash K and Zhao H 2016 Designs of blue and green light-emitting diodes based on type-II InGaN-$ZnGeN_2$ quantum wells *J. Appl. Phys.* **120** 103102
[11] Zhu L, Maruska P, Norris P, Yip P and Bouthillette L 1999 Epitaxial growth and structural characterization of single crystalline $ZnGeN_2$ *MRS Internet J. Nitride Semicond. Res.* **4** 149–54
[12] Misaki T, Tsuchiya K, Sakai D, Wakahara A, Okada H and Yoshida A 2003 Growth and characterization of $ZnGeN_2$ by using remote-plasma enhanced metalorganic vapor phase epitaxy *Phys. Status Solidi* c **n/a** 188–91
[13] Misaki T, Wakahara A, Okada H and Yoshida A 2004 Epitaxial growth and characterization of $ZnGeN_2$ by metalorganic vapor phase epitaxy *J. Cryst. Growth* **260** 125–9
[14] Osinsky A, Fuflyigin V, Zhu L D, Goulakov A B, Graff J W and Schubert E F 2000 New concepts and preliminary results for SiC bipolar transistors: $ZnSiN_2$ and $ZnGeN_2$ heterojunction emitters *Proc. 2000 IEEE/ Cornell Conf. on High Performance Devices (Cat. No.00CH37122)* pp 168–72
[15] Karim M R, Dinushi Jayatunga B H, Zhang K, Zhu M, Hwang J, Kash K and Zhao H 2022 Band structure engineering based on InGaN/$ZnGeN_2$ heterostructure quantum wells for visible light emitters *Cryst. Growth Des.* **22** 131–9
[16] Karim M R, Noesges B A, Jayatunga B H D, Zhu M, Hwang J, Lambrecht W R L, Brillson L J, Kash K and Zhao H 2021 Experimental determination of the valence band offsets of $ZnGeN_2$ and $(ZnGe)_{0.94}Ga_{0.12}N_2$ with GaN *J. Phys. D: Appl. Phys.* **54** 245102
[17] Karim M R, Jayatunga B H D, Zhu M, Lalk R A, Licata O, Mazumder B, Hwang J, Kash K and Zhao H 2020 Effects of cation stoichiometry on surface morphology and crystallinity of $ZnGeN_2$ films grown on GaN by metalorganic chemical vapor deposition *AIP Adv.* **10** 065302

[18] Karim M R, Jayatunga B H D, Feng Z, Kash K and Zhao H 2019 Metal-organic chemical vapor deposition growth of $ZnGeN_2$ Films on sapphire *Cryst. Growth Des.* **19** 4661–6
[19] Melamed C L, Pan J, Mis A, Heinselman K, Schnepf R R, Woods-Robinson R, Cordell J J, Lany S, Toberer E S and Tamboli A C 2020 Combinatorial investigation of structural and optical properties of cation-disordered $ZnGeN_2$ *J. Mater. Chem.* **8** 8736–46
[20] Tellekamp M B, Miller M K, Rice A D and Tamboli A C 2022 Heteroepitaxial $ZnGeN_2$ on AlN: growth, structure and optical properties *Cryst. Growth Des.* **22** 1270–5
[21] Tellekamp M B, Miller M K, Zhou L and Tamboli A 2023 Structure, defects and optical properties of commensurate GaN/$ZnGeN_2$/GaN double heterojunctions *J. Mater. Chem.* **11** 13917–23
[22] Storm D F, Katzer D S, Meyer D J and Binari S C 2012 Oxygen incorporation in homoepitaxial N-polar GaN grown by radio frequency-plasma assisted molecular beam epitaxy: mitigation and modeling *J. Appl. Phys.* **112** 013507
[23] Moseley M, Billingsley D, Henderson W, Trybus E and Doolittle W A 2009 Transient atomic behavior and surface kinetics of GaN *J. Appl. Phys.* **106** 014905
[24] Thompson K, Lawrence D, Larson D J, Olson J D, Kelly T F and Gorman B 2007 In situ site-specific specimen preparation for atom probe tomography *Ultramicroscopy* **107** 131–9
[25] Giannuzzi L A, Drown J L, Brown S R, Irwin R B and Stevie F A 1998 Applications of the FIB lift-out technique for TEM specimen preparation *Microsc. Res. Tech.* **41** 285–90
[26] Gorman B P, Diercks D, Salmon N, Stach E, Amador G and Hartfield C 2008 Hardware and techniques for cross-correlative TEM and atom probe analysis *Microsc. Today* **16** 42–47
[27] Diercks D R and Gorman B P 2018 Self-consistent atom probe tomography reconstructions utilizing electron microscopy *Ultramicroscopy* **195** 32–46
[28] Sands T, Palmstrøm C, Harbison J, Keramidas V, Tabatabaie N, Cheeks T, Ramesh R and Silberberg Y 1990 Stable and epitaxial metal/III-V semiconductor heterostructures *Mater. Sci. Rep.* **5** 99–170
[29] Reshchikov M A and Morkoç H 2005 Luminescence properties of defects in GaN *J. Appl. Phys.* **97** 061301
[30] Cordell J J, Tucker G J, Tamboli A and Lany S 2022 Bandgap analysis and carrier localization in cation-disordered $ZnGeN_2$ *APL Mater.* **10** 011112
[31] Mancini L *et al* 2014 Composition of wide bandgap semiconductor materials and nanostructures measured by atom probe tomography and its dependence on the surface electric field *J. Phys. Chem.* C **118** 24136–51
[32] Hageman P, Schaff W, Janinski J and Liliental-Weber Z 2004 n-type doping of wurtzite GaN with germanium grown with plasma-assisted molecular beam epitaxy *J. Cryst. Growth* **267** 123–8
[33] Bogusławski P and Bernholc J 1997 Doping properties of C, Si and Ge impurities in GaN and AlN *Phys. Rev.* B **56** 9496–505